

## AN EFFICIENT METHOD FOR AUTOMATIC LAND- COVER CLASSIFICATION WITH HIGH RESOLUTION IMAGERY USING THE OBJECT-ORIENTED PARADIGM

Bo Zhao <sup>1\*</sup>, Jürgen Pilz <sup>2</sup>, Fan Yang <sup>3,4,5</sup>, Junping Shen<sup>1</sup>

<sup>1</sup> Advanced Algorithm Research Division, Beijing PIESAT Information Technology Co., Ltd, 100195 Beijing, China.

<sup>2</sup> Institute of Statistics, Alpen-Adria-Universität Klagenfurt, 9020 Klagenfurt, Austria.

<sup>3</sup> Beijing Institute of Geology for Mineral Resources, Beijing, China.

<sup>4</sup> Key Laboratory of Geochemical Cycling of Carbon and Mercury in the Earth's Critical Zone, Institute of Geophysical and Geochemical Exploration, Chinese Academy of Geological Sciences, Langfang, China.

<sup>5</sup> State Key Laboratory of Ore Deposit Geochemistry, Institute of Geochemistry, Chinese Academy of Sciences, Guiyang, China.

**Correspondence:** xqqelove@yahoo.com (B. Zhao)

E-mail: [xqqelove@yahoo.com](mailto:xqqelove@yahoo.com); [Juergen.Pilz@aau.at](mailto:Juergen.Pilz@aau.at); [yangfan@igge.cn](mailto:yangfan@igge.cn); [shenjunping@piesat.com](mailto:shenjunping@piesat.com)

**KEY WORDS:** Land Cover; Classification; Divergence; Interpolation; Automation

**ABSTRACT:** To classify an image, traditional classifiers depend mainly on the spectral and/or textural distinctions between different land-cover units, while this study attempts to explore the properties of statistical distinction. We present a novel algorithm for imagery classification that achieves high accuracy, automation and efficiency. Based on object-oriented image analysis, it exploits the advantages of JSD (Jensen-Shannon Divergence) using a multi-step approach, and the objective is not to reclassify an image, but to refine or update the existing land-cover classification results by comparing the pairwise JSD value (namely similarity) between different image segments. Finally, the similar/homogeneous segments will be confirmed as their original class labels, while the inhomogeneous/dis-similar segments will be masked out with an appropriate threshold on the similarity image and be relabeled. We have systematically evaluated the algorithm by running it on the basis of the existing GIS database, which indicated the good performance of it.

### 1. INTRODUCTION:

As the accuracy and sensitivity of remote sensing (RS) satellites improve, there is increasing emphasis on the need for land cover products derived from high-resolution RS data. As the per-pixel based methods cannot effectively solve the high spectral variation problem within the same land cover, there has been a very rapid growth in the use of object-oriented imagery analysis ever since its documented introduction in late 1990s. The first step of this method is the grouping of spatially contiguous pixels with similar spectral/textural characteristics into meaningful objects, which is a process often termed segmentation (Laliberte et al. 2004); once the objects are formed, the next step is to assign appropriate labels to them by using a supervised or ruleset-based classifier.

A problem with this framework is that the massive amount of data of the improved sensor may pose increasing complexities to a degree that the existing object-oriented methods may be insufficient to cope with. For example, the spectral, or even textural, confusion among different land covers is a common factor contributing to the difficulty in the automatic production of high-quality classifications, and one important reason is that the spectral bands in high spatial resolution imagery have only visible bands and one near-infrared band, and lack diagnostic shortwave-infrared

bands (Navulur et al. 2013), so that in many cases manual editing becomes necessary and may be the only way to improve the thematic mapping performance. However, the theoretical framework of this method has been well established, and seemingly there is little room for substantial improvement (Blaschke, 2010), so greater weight is better to put on the image analysis or interpretation strategy. For example, improved classification is obtained by separately performing segmentation and classification on different image data, and combining the results afterwards (Marcheggiani et al. 2009), e.g. the high-resolution image can be used to identify and delineate suitable segments, while the multi-spectral image used as a reference for the segment classification.

Object-based classification approaches commonly rely on object-level summary statistics, such as mean and standard deviation of the reflectance values within each imagery object. Such summary measures provide one value per band for each object to describe its data central tendency or dispersion. Standard object-based classifiers work with only object-level summary statistics of the reflectance values and do not sufficiently exploit within-object reflectance pattern which is often not normal but multi-peaked. To address this problem, Sridharan and coworkers (2013) presented a Fuzzy-Kolmogorov-Smirnov based classifier to provide an object-to-object matching of the empirical cdf (Cumulative Distribution Function) of the reflectance values of each object to a theoretical counterpart, also it derives a fuzzy membership grade to each class. This is a rather innovative idea, but people have to manually select and label the training samples in order to construct the reference cdfs. This research is in the spirit of Sridharan et al (2013). First, to reduce the human intervention, it is better to run the Kolmogorov-Smirnov Test between the imagery segments themselves, rather than between image segments and the labeled training dataset. Second, at the suggestion of Polzehl & Spokoiny (2006), it is better to measure the similarity of any two segments by introducing the Kullback-Leibler (KL) divergence, which is a measure of how one probability distribution is different from another, or from the reference probability distribution. Rather than just having the probability distribution  $p(x)$  which is usually unknown in practical scenarios, it adds in an approximating distribution  $q(x)$ , and for discrete probability distributions  $p$  and  $q$  defined on the same probability space, which is defined to be:  $D_{KL}(p||q)=H(p)-H(p, q)$ , where  $H(p)=-\sum_x p(x) \log p(x)$  is the entropy of  $p(x)$  and  $H(p, q)=-\sum_x p(x) \log q(x)$  is the cross entropy of  $p(x)$  and  $q(x)$ . The KL model is not symmetric because  $D_{KL}(p||q) \neq D_{KL}(q||p)$ , so it is not always a good metric, and instead the Jensen-Shannon divergence is commended in practice (see context described later).

There are many automatic classifiers which are rule-/knowledge-based, or based on supervised learning depending on reference maps to improve the accuracy of the classification process; one can find the work presented in, but not limited to, Walter (2004), Nussbaum et al. (2006), Inglada (2007), etc. Unlike them, here we will construct a similarity-based classifier which is fully automated and independent of any training data to save both time and labor to build or update the land cover classification. Use of high resolution images facilitates higher accuracy, but in turn increases the computational and problem complexity due to artifacts, hence the proposed algorithm is required to incorporate the existing land cover product (generated automatically or manually) and update it, rather than reclassifying it. To this end, the remainder of this article is organized as follows: Section II reviewed the KL divergence theory and introduced an available model for measuring the similarity between the imagery patches (segments); Section III suggested several criteria for the development of systems for identifying different land cover classes; Section IV evaluated the accuracy and efficiency of the proposed algorithm; and Section V concluded the research by pointing out the future directions.

## 2. METHODOLOGY

This algorithm is a complex multi-step procedure that gets involved in the development of several different methodologies and datasets, and the details of each step are given below. Based on MATLAB, Aim of the algorithm is to exclude and then reclassify the dissimilar /inhomogeneous parts of the roughly classified imagery.

(1) Data Input and Pre-processing:

The input data include: the high-resolution RS imagery under detection and the segmented image layer (in Raster format). The relevant pre-processing may involve geometric correction, atmospheric correction, Pan sharpening, reprojection, etc.

(2) The Preliminary Classification:

It should be noted that the objective of this study is not to classify an image scene independently, but to update or improve the existing classification results that can be generated automatically using the unsupervised classifier (e.g. Neural Network Clustering). However, as shown in Fig. 1, such a preliminary classification procedure does not assure to follow detailed and well-structured land cover nomenclature, if it is not performed by a customized learning system; and the interpretation accuracy may diminish in areas with highly heterogeneous landscapes. Therefore, it is better to run the algorithm flow on the basis of the existing GIS database, so that it classifies not single pixels but groups of pixels that represent existing objects in the database.

(3) Image Mask:

The output of (2) is a shapefile with unlabeled class attributes, which is the first step of scene understanding. On this basis, the input imagery will be binarized to become mask images, and each of them corresponds to a particular land cover type (class).

(4) The Comprehensive Image Feature:

A good enhancement operator can significantly reduce (or increase) the brightness of dark (or bright) object structures in the original image, but has no effect on non-target pixels. However, which of the numerous possible features (imagery enhancing methods) are most characteristic for calculation of JSD? The PCA (principal component analysis) image or grayscale image is preferred in this step, for in which the original multi-spectral characteristics can be integrated by removing the redundant information across the bands. In other words, it gives a comprehensive image enhancement, rather than anything specific (e.g. the image enhancement of buildings, vegetation, or waters). It is believed that the application of the principal component transformation to correlated RS data will result in an uncorrelated dataset and will effectively separate redundancy from the input imagery. Accordingly, this procedure can guarantee the stability of the classification algorithm and can improve the classification efficiency/accuracy.

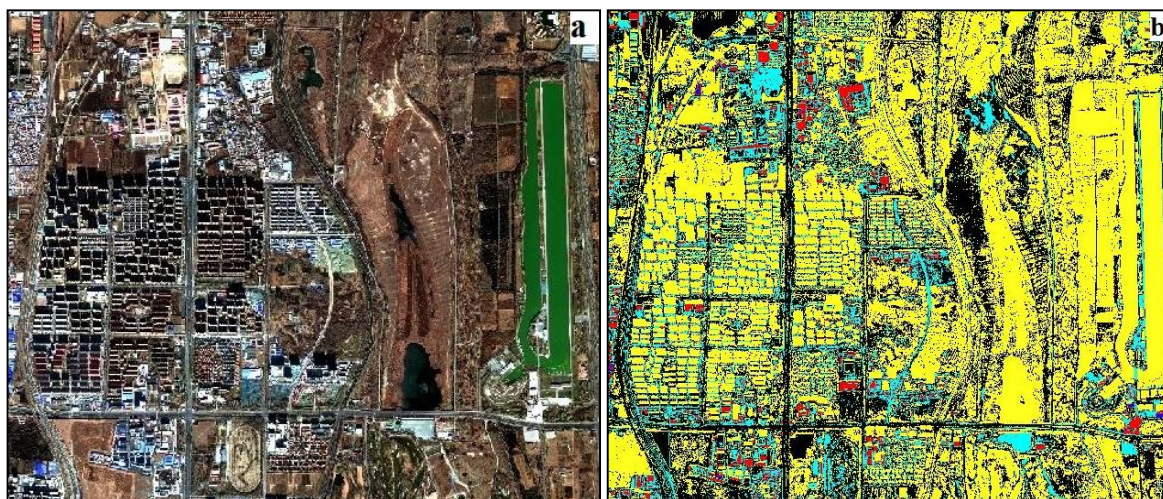


Figure 1 a) is the Original Image in North Beijing of China (the GF-2 satellite image, 0.8m resolution after fusion, and Band 3, 2, & 1 in RGB); b) is the Relevant Classification Result Generated by the Neural Network Clustering Algorithm which is among the most advanced unsupervised classification algorithms, where different colors represent different land-cover classes.

(5) The Image Segmentation and P-Q Pairing:

The purpose of object-oriented image segmentation is to subdivide an image into different segments that

correspond to real-world objects in the terrain. As seen in Fig.2, suppose there are  $j$  segments being labelled as Class  $i$  ( $i, j=1, 2, \dots, n$ ) after the unsupervised classification, and keep  $i$  unchanged, then there will be  $j^2$  P-Q combinations available for calculation of JSD, producing a  $j \times j$  JSD matrix. Here P and Q represent the dataset  $\{p_{ijk}\}$  and  $\{q_{ijk}\}$ , respectively, where  $k=1, 2, \dots$ , and the element  $p_{ijk}$  or  $q_{ijk}$  signifies the  $k$ -th pixel value in Segment  $j$  and Class  $i$ .

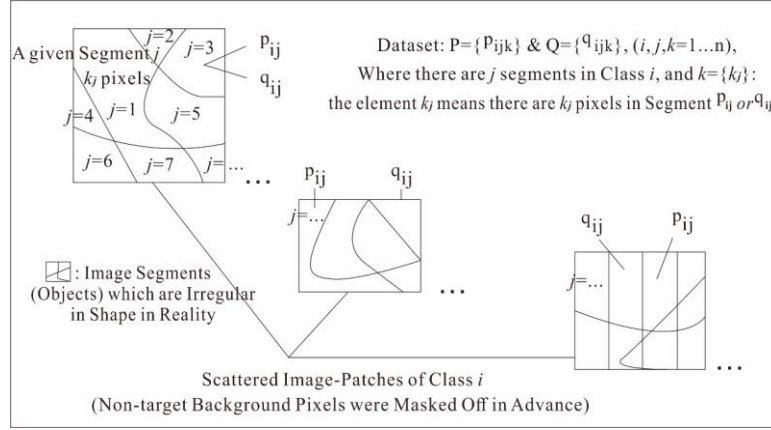


Figure 2 The P-Q Pairing and Calculation of JSD

#### (6) Data Interpolation and Compression:

In Fig. 2, image segments usually come in many different shapes, areas and sizes (pixel numbers). Suppose there is a pair of segments  $p_j$  and  $q_l$  ( $j \neq l$ ) in Class  $i$ , and the size of  $p_j > q_l$ , then the interpolation (or compression) algorithm must be applied to  $q_l$  (or  $p_j$ ) in order to let them have the same size. Otherwise, JSD cannot be determined.

Here the fractal interpolation algorithm is preferred because fractal geometry has unique advantages for a broad class of data-modeling problems, especially for geographical objects and patterns. Unlike many other algorithms (e.g., the Lagrange or Spline interpolation), fractal interpolation which is based on IFS (Iterated Function System (Wittenbrink, 1995)) can give satisfactory results because it does not assume smoothness.

Consider a two-point interval  $I_i = [x_{j-1}, x_j]$ , let Transformation  $L_j: I_i \rightarrow I_j$  ( $j=0, 1, 2, \dots, N$ ), where  $L_j(x_0) = x_{j-1}$ ,  $L_j(x_N) = x_j$ , and let Transformation  $F_j: K \subset 1 \times \mathbb{R} \rightarrow [a, b]$  ( $a$  and  $b$  are continuous), where  $F_j(x_0, y_0) = y_{j-1}$ ,  $F_j(x_N, y_N) = y_j$ . Define the affine transformation  $W_j(x, y) = (L_j(x), F_j(x, y))$ , which has a unique attractor  $G$ .  $G$  is the graph of a continuous interpolation function  $f: I \rightarrow [a, b]$ , which meets the condition  $f(x_i) = y_i$ ,  $i=0, 1, 2, \dots, N$ . On this basis, consider the IFS  $\{R^2: W_n, n=1, 2, \dots, N\}$ , where  $W_n$  is presented as follows:

$$w_n \begin{bmatrix} x \\ y \end{bmatrix} = \begin{bmatrix} a_n & 0 \\ c_n & d_n \end{bmatrix} \begin{bmatrix} x \\ y \end{bmatrix} + \begin{bmatrix} e_n \\ f_n \end{bmatrix}, \quad (1)$$

$$\text{Where } w_n \begin{bmatrix} x_0 \\ y_0 \end{bmatrix} = \begin{bmatrix} x_{n-1} \\ y_{n-1} \end{bmatrix}, \quad w_n \begin{bmatrix} x_N \\ y_N \end{bmatrix} = \begin{bmatrix} x_n \\ y_n \end{bmatrix}, \quad (2)$$

$$a_n = \frac{x_n - y_n}{L}, \quad e_n = \frac{x_N x_{n-1} - x_0 x_n}{L}, \quad c_n = \frac{y_n - y_{n-1} - d_n (y_N - y_0)}{L}, \quad (3)$$

$$\text{And } f_n = \frac{x_N y_{n-1} - x_0 y_n - d_n (x_N y_0 - x_0 y_N)}{L} \quad (4)$$

Here the  $d_n < 1$  is a free parameter, also known as the vertical scale factor, which makes IFS a convergent function. These are how the fractal interpolation works.

In order to keep the derived dataset as close to the original one as possible, we prescribe that the data interpolation is conducted only for the segments with area (pixel number  $k_j$ ) less than the median level. Likewise, suppose there are two column vectors  $p_j$  &  $q_l'$ , where  $q_l'$  is the interpolated result of  $q_l$ , and the size of  $p_j > q_l'$ , then

the data compression (downsampling) must be conducted on  $p_j$ , which is readily implemented in e.g., MATLAB. Aim of these calculations is to make each of the P-Q pairs generated in Step (5) the same size and available for calculation of JSD.

(7) Calculation of JSD

The JS divergence which is defined as below is based on the KL divergence, with notable but useful differences, including that it is symmetric and it always has a finite value –ranging between [0, 1]. A JS divergence (JSD) of 0 indicates that the two distributions in question are identical. The greater JSD is, the more inhomogeneous/dissimilar is the two datasets under comparison.

$$JSD(p||q)=\frac{1}{2} D_{KL}(p||(p+q)/2)+ \frac{1}{2} D_{KL}(q||(p+q)/2), \tag{5}$$

Where  $JSD = JSD_{ij}$ ,  $p = \{p_{ijk}\}$  and  $q = \{q_{ijk}\}$ . (6)

Here, JSD is used to measure the (dis)similarity between each image segment’s statistical distributions, and it is estimated based on the PCA or grayscale image.

(8) The Pairwise JSD Matrix and the Similarity Assignment:

Following Step (4)-(6) and keeping Class  $i$  unchanged, we can obtain a  $j \times j$  JSD matrix; and as exhibited in Fig.3, the subsequent operations are fourfold as follows:

1. Label the original JSD values as 1 (true) if they are equal to or smaller than a pre-defined threshold (T), otherwise, label them as 0 (false).
2. Calculate the summation of row elements from top to bottom in the matrix, and note the result in each line by  $N_j$ , where  $j=1, 2, \dots$  is the image-segment number.
3. Find the row ( $j_0$ ) with the maximum  $N_j$  value, and then, assign each segment of Class  $i$  the original JSD value at row  $j_0$  and column 1 to  $j$  of the matrix. If  $j_0$  is not unique, the one corresponding to the maximum segment  $j$  area will be selected.
4. From the above, the Similarity contour of any given Class  $i$  can be sketched.
5. Repeat the above operations until the maximum  $i$  is reached.

The similarity assignment is conducted based on the assumption/(fact) that (1): most of the elements in datasets P and Q in a given, although unlabeled, Class  $i$  should have relatively-high statistical similarities to each other; and 2) the number of them must be big, because otherwise they cannot form a realistic ground feature. To balance these issues, the maximum  $N_j$  value in Fig. 3 is considered here. In addition, through extensive experimentation we have determined value of  $T=0.30\sim 0.50$  gives the best results, which is sensitive to the separation of one object from background.

		Segment No.						Sum	
		Q	1	2	3	4	...		j
Segment No.	P								
	1	1	0	0	0	...	1	$N_1$	
	2	0	1	1	1	...	0	$N_2$	
	3	0	1	1	0	...	1	$N_3$	
	4	0	0	0	0	...	1	$N_4$	
	...	...	...	...	...	...	...	Maximum	
	j	1	0	0	0	...	1	$N_j$	

Note: "1" means  $JSD \leq T$ ; "0" means  $JSD > T$ ;  
T: A given threshold;  $N_j$  is the summation of the row elements.

Figure 3 Analysis of the JSD Matrix (simulated data) in which the Original JSD values were substituted by Boolean numbers.

(9) Thresholding and Land Cover Classification

Setting appropriate thresholds is essential to eliminate the dissimilar parts of an otherwise homogenous image. We assumed that the number of misclassified segments labelled as class  $i$  in step (2) is very small compared with the number of all GIS objects in this class, but it appeared hard to find an empirical threshold value that performed the best over the whole imagery. Here the multifractal-thresholding algorithm which is dynamic is considered (Wang et al. 2018). It quantifies the power-law relationship between  $JSD_{ij}$  values and their cumulative summation in the following way:

$$N(\geq r) = Cr^{-D} \quad (r > 0) \tag{7}$$

Where  $r$  is the obtained  $JSD_{ij}$  value, and  $N(\geq r)$  denotes the summation (or frequency) of pixel values larger than or equal to a given  $r$ .  $C > 0$  is a proportionality coefficient, and the exponent  $D$  is known as the fractal dimension.

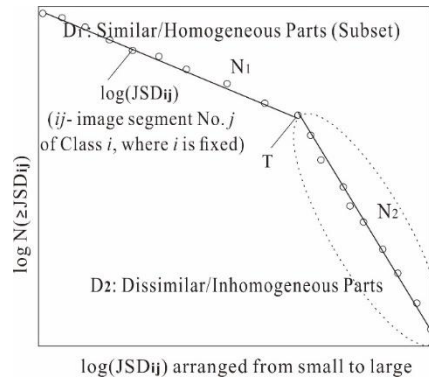


Figure 4 Fractal Schema of A Given Class' Similarity Image  
 Note:  $N_1/N_2$  is the proportion that image segments falling within  $D_1/D_2$ , respectively, are of the total segments, and in most cases  $N_1 > N_2$ .

Mathematically, a number of straight-line segments (namely scaleless intervals) can be derived from the power-law equation on the log-log paper. It aims to cluster a dataset into most similar groups in the same segment and most dissimilar groups in different segments. Here in this step, they are customarily classified into two segments ( $D_1$  and  $D_2$ ) as illustrated in Figure 4, and  $T$  is selected as the threshold value for defining the dissimilar parts (subset) of a given class  $i$ .

(10) Reclassification of the Remaining Ambiguous Segments:

“Unconfirmed” Segment No.

P	1	4	7	24	...	j
JSD of P-QQ <sub>1</sub>	1.0	0.4	0.1	0.5	...	0.9
JSD of P-QQ <sub>2</sub>	0.1	0.6	0.2	0.7	...	0.7
JSD of P-QQ <sub>3</sub>	0.3	0.1	0.7	0.0	$i_0$	0.6
JSD of P-QQ <sub>4</sub>	0.5	0.3	0.2	0.9	...	0.2
...	$i_0$	$i_0$	$i_0$	...	...	...
JSD of P-QQ <sub>i</sub>	1.0	0.4	0.1	0.0	$i_0$	1.0

Figure 5 the resulting P-QQ<sub>i</sub> JSD matrix.

After executing step (7)-(9), the categorization of segments within the similar parts  $D_1$  of Fig.4 is confirmed as  $i$ ,

while others within  $D_2$  will be reclassified as below:

1. For a given Class  $i$ , select the segment falling within  $D_1$  with the maximum area as the reference dataset ( $QQ_i$ , equivalent to  $Q$ ), where  $i$  is the known Class number.

2. Use  $JSD_{ij}$  to quantify the similarity between each of the “unconfirmed” segments and  $QQ_i$  (unlike  $Q$ ,  $QQ_i$  is fixed here), and the output is visualized in Fig. 5.

3. In Fig.5, for a given Class  $i$  or  $QQ_i$ , find the column ( $i_0$ ) with the minimum  $JSD$  value, and then, reclassify the corresponding segment ( $P_j$ ) as  $i_0$ . If  $i_0$  is not unique, randomly select one of them as the class label.

4. Repeat the above operations until the maximum  $i$  is reached.

(11) Thematic Mapping:

As many, if not most, of the image segments are not of interest when the focus is on segments labelled as Class  $i$ , so the results obtained at each step will be combined to generate a thematic map of several land-cover classes.

### 3. EXPERIMENTAL RESULTS

#### 3.1 Data Preparation

Fig. 6 gives the testing GF-2 image after pre-processing (extents:  $N30^{\circ}47'18'' \sim N 30^{\circ}48'05''$  and  $E104^{\circ}38'13'' \sim E104^{\circ}39'28''$ ). The GF-2 sensor has four spectral bands from the visible light to near-infrared with 0.80 m spatial resolution after fusing with the panchromatic band. The corresponding GIS database, which was built up by China Land Surveying and Planning Institute in early 2016, has been derived from manually digitizing the outlines of different land-cover polygons and attribute descriptions in the RS image. The object-oriented multiresolution segmentation layer was generated based on PIE-SIAS v5.0. The study terrain is partly forested, and it represents the heterogeneous characteristics of land use status in south-western China, which consists of e.g., roads of different widths, free-standing waters, residential areas, rangelands, bare soils, paddy fields, shrub lands, as well as a variety of agricultural systems (e.g. fallow land, irrigated or rain-fed field crops, orchards...).



Figure 6. The Input High-Resolution Image (band 321 in RGB)

#### 3.2 Results of Step (3)-(9)

Using the first principal component (PC1) imagery with the greatest amount of information (highest sum of standard deviations) as the comprehensive feature, Step (3)-(9) results in the exclusion of pixels with the class-labels unconfirmed. In Figure 7, about 65.89% of the pixels fenced off by different segments remain, and 34.11% originally labelled as “water”, “farmland”, “building”, etc., are ruled out because of a high level of spectral dissimilarity caused

by land utilization change or false alarms.

For waters, about 64.62% of the pixels originally labelled as “water” remain, and 35.38% are ruled out, and as shown in Fig. 8a, most of them correspond to vegetation or waters with phytoplankton. Nevertheless, confusion of similarity among different land cover units is also possible, in Fig. 8a several objects reflecting the dried lake bed are mistaken for waters, and there may be no solution to address this problem. Similar phenomena had been observed by Tang et al. (2011) when they conducted object-oriented change detection based on the Kolmogorov-Smirnov test. As shown in Figure 8b, for forest, the deleted segments correspond mainly to bare lands, roads, and the forests themselves, and 55.53% of the pixels originally labelled as “forest” remain, which are, however, mixed in with several patches of bare earth. In Fig. 8c, 59.28% of the pixels originally labelled as “building” remain, along with only a few false alarms. In Figure 8d, 71.19% of the pixels originally labelled as “farmland” are confirmed, and 28.81% are deleted because of their low levels of similarity, which correspond to roads, bare earth, waters, and etc. In the same manner, the similar parts of other classes e.g. Road (Fig.8e), Orchard (Fig. 8f), Grass Land, and so on were separated out.



Figure 7 The Similar Parts Of Figure 6. The black background is masked, which corresponds to the spectrally dissimilar/inhomogeneous pixels of the known classes {i}.

### 3.3 Results of Step (10)-(11)

In Fig. 7, 34.11% of the pixels are masked off and need to be reclassified (by the way, the remaining segments can be very good training samples for machine learning). Tab.1 gives the JSD matrix of the “unconfirmed” segments. In most cases the minimum JSD of each row corresponds to a unique class label, and this label is the label to be assigned to the corresponding segment. As shown in Fig. 9, the extracted water features, built-up areas, farmlands and so on were combined to produce the land cover classification thematic map. The overall accuracy of the classification is 82% (the overall Kappa coefficient is 0.714) -- 5% higher than the accuracy of the reference shapefile. The overall accuracy of Class Water, Building, Forest, Orchard, Grassland, Road, Farmland, and Others are 73%, 84%, 65%, 80%, 97%, 88%, and 91%, respectively, which indicates a satisfactory result in general that can be well validated with the input image and implies the usefulness of the algorithm.

## 5. Discussion and Conclusion

We have presented a hybrid algorithm to automatically classify the high resolution imagery. The approach exploits the properties of JSD (acting as the spectral similarity measurement) using a multi-step approach. The main steps in our algorithm are: rough classification, image segmentation, image masking, data interpolation or compression, calculating the pairwise JSD matrix, thresholding and doing classification, and etc. The algorithm can work fully automatically because all information for the classification is derived from a roughly classified thematic layer or the

already existing GIS database; and in order to assure accuracy, we assumed that the number of misclassified segments labelled as a given class is very small compared with the number of all GIS objects in this class. It is noteworthy that the theoretical basis of the proposed algorithm is quite different from the traditional ruleset-/knowledge- oriented or supervised learning-based classifiers, the issue faced in this algorithm is not to construct an object-level classifier, but to quantify the pairwise similarity between within-class segments/objects, which involves a set of statistical operations (e.g. interpolation, compression, and calculation of JSD) for the within-object pixel values. It is expected to provide a more refined image land-cover classification and intelligently select the most informative training samples used for deep learning. However, we have to accept that this type of algorithm is time- consuming due to iteration computation.

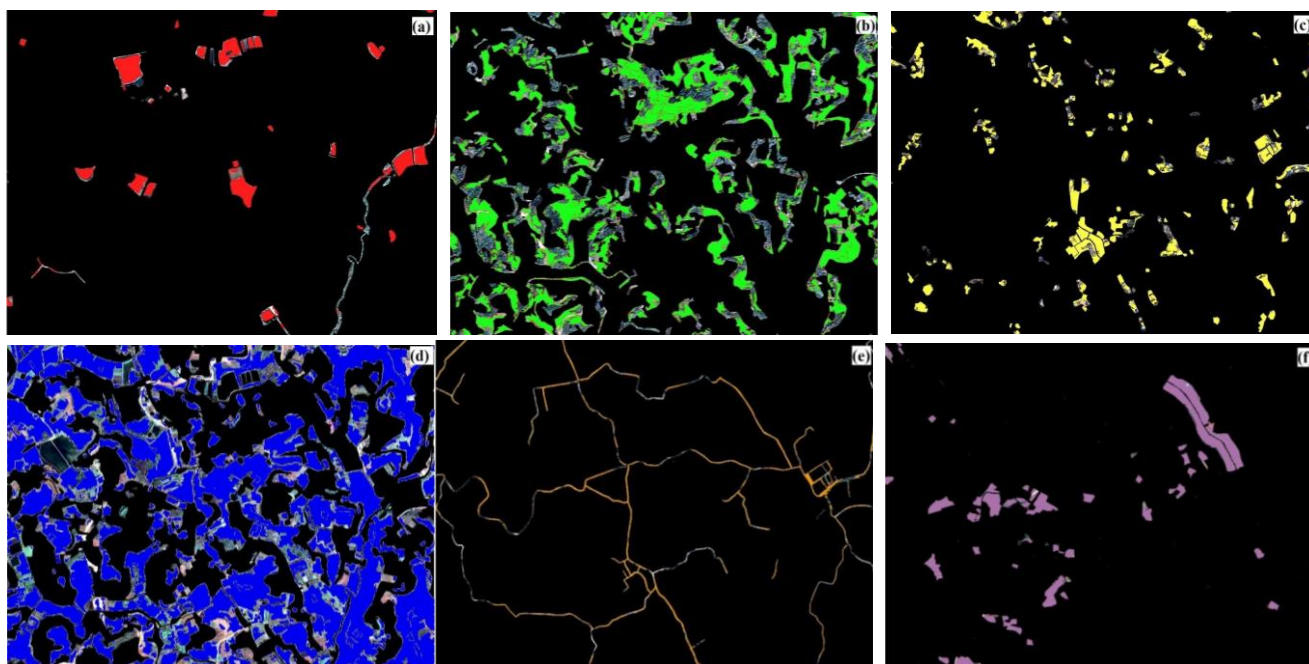


Figure 8 The Similar Parts (Colored Patches) of Class (a) “Water”, (b) “Forest”, (c) “Building”, (d) “Farmland”, “Road”, and “Facility agricultural land”, which are overlaid on the natural color image background, namely the masked images derived from Step (3). The black background is masked according to the Class we are focusing on. Note that for Class “water”, the log (JSD) versus log (N) plot was divided into three segments, and thus there are two thresholds produced. Here the one with smaller JSD is selected as the threshold distinguishing the “similar” and “dissimilar” parts. This is because the water area decreased significantly during the study period.

Table 1 excerpt of the P-QQ JSD matrix

Seg. No. Class Label	Forest	Water	Building	Farmland	Orchard	Grassland	Road	Others
1	0.00153	<b>0.00017</b>	0.00316	0.00059	0.00035	0.00027	0.00039	0.00719
2	NaN	NaN	NaN	NaN	NaN	NaN	NaN	NaN
3	0.00284	<b>0.00037</b>	0.00466	0.00067	0.00120	0.00117	0.00053	0.00815
4	0.00177	0.00060	0.00320	0.00075	0.00083	0.00081	<b>0.00051</b>	0.00719
5	NaN	NaN	NaN	NaN	NaN	NaN	NaN	NaN
...	...	...	...	...	...	...	...	...

Note: FAL represents “Facility Agricultural Land”, NaN represents the null value.

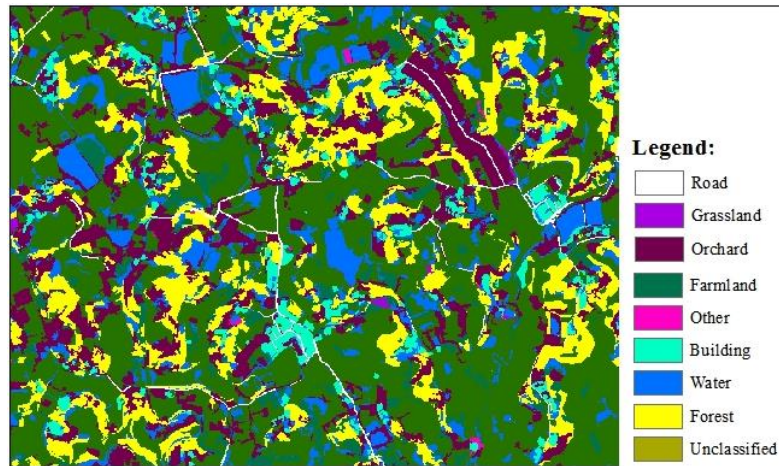


Fig. 9 the classification thematic map

## REFERENCE

- Blaschke, T. 2010. Object based image analysis for remote sensing. *ISPRS journal of photogrammetry and remote sensing*, 65(1), pp. 2-16.
- Inglada, J. 2007. Automatic recognition of man-made objects in high resolution optical remote sensing images by SVM classification of geometric image features. *ISPRS journal of photogrammetry and remote sensing*, 62(3), pp. 236-248.
- Laliberte, A. S., Rango, A., Havstad, K. M., Paris, J. F., Beck, R. F., McNeely, R., & Gonzalez, A. L. 2004. Object-oriented image analysis for mapping shrub encroachment from 1937 to 2003 in southern New Mexico. *Remote Sensing of Environment*, 93(1-2), pp. 198-210.
- Marcheggiani, E., Galli, A., Bernardini, A., Malinverni, E. S., & Zingaretti, P. (2009, May). Selection criteria of training set for optimal land cover discrimination with a view to automatic segmentation. In *Remote Sensing for a Changing Europe: Proceedings of the 28th Symposium of the European Association of Remote Sensing Laboratories*, Istanbul, Turkey, 2-5 June 2008 (p. 284). IOS Press.
- Navulur, K., Pacifici, F., & Baugh, B. 2013. Trends in optical commercial remote sensing industry [industrial profiles]. *IEEE Geoscience and Remote Sensing Magazine*, 1(4), pp. 57-64.
- Nussbaum, S., Niemeyer, I., & Canty, M. J. (2006, July). SEATH—a new tool for automated feature extraction in the context of object-based image analysis. In *1st International Conference on Object-based Image Analysis (OBIA)*. Salzburg: Austria.
- Polzehl, J., & Spokoiny, V. 2006. Propagation-separation approach for local likelihood estimation. *Probability Theory and Related Fields*, 135(3), pp. 335-362.
- Sridharan, H., & Qiu, F. 2013. Developing an object-based hyperspatial image classifier with a case study using WorldView-2 data. *Photogrammetric Engineering & Remote Sensing*, 79(11), pp. 1027-1036.
- Tang, Y., Zhang, L., & Huang, X. 2011. Object-oriented change detection based on the Kolmogorov–Smirnov test using high-resolution multispectral imagery. *International journal of remote sensing*, 32(20), pp. 5719-5740.
- Walter, V. 2004. Object-based classification of remote sensing data for change detection. *ISPRS Journal of photogrammetry and remote sensing*, 58(3-4), pp. 225-238.
- Wang, R., Lin, J., Zhao, B., Li, L., Xiao, Z., & Pilz, J. 2018. Integrated Approach for Lithological Classification Using ASTER Imagery in a Shallowly Covered Region—The Eastern Yanshan Mountain of China. *IEEE Journal of Selected Topics in Applied Earth Observations and Remote Sensing*, 11(12), pp. 4791-4807.
- Wittenbrink, C. M. (1995, October). IFS fractal interpolation for 2D and 3D visualization. In *Proceedings of the 6th conference on Visualization'95* (p. 77). IEEE Computer Society.